Realizing time crystals in discrete quantum few-body systems

R. E. Barfknecht,[1,2,*] S. E. Rasmussen,[2,†] A. Foerster,[1,‡] and N. T. Zinner[2,3,§]
[1]*Instituto de Física da UFRGS, Avenido Bento Gonçalves 9500, Porto Alegre, Rio Grande do Sul, Brazil*
[2]*Department of Physics and Astronomy, Aarhus University, Ny Munkegade 120, Denmark*
[3]*Aarhus Institute of Advanced Studies, Aarhus University, DK-8000 Aarhus C, Denmark*

(Received 28 July 2018; revised manuscript received 17 November 2018; published 11 April 2019)

The exotic phenomenon of time-translation-symmetry breaking under periodic driving—one of the main features of the so-called time crystals—has been shown to occur in many-body systems even in clean setups where disorder is absent. In this work, we propose a realization of this effect in few-body systems, both in the context of trapped cold atoms with strong interactions and of a circuit of superconducting qubits. We show how these two models can be treated in a fairly similar way by adopting an effective spin-chain description, to which we apply a simple driving protocol. We focus on the response of the magnetization in the presence of imperfect pulses and interactions, and show how the results can be interpreted, in the cold atomic case, in the context of experiments with trapped bosons and fermions. Furthermore, we provide a set of realistic parameters for the implementation of the superconducting circuit.

DOI: 10.1103/PhysRevB.99.144304

I. INTRODUCTION

Recent developments in theory and experiments with time-dependent quantum mechanical setups have consolidated the concept of the *discrete time crystal*, a system that presents spontaneous breaking of time-translation symmetry. The original proposals, both in the quantum [1] and classical [2] regimes, suggested the possibility of a system exhibiting a periodic dynamical behavior in its lowest energy state [3]. This possibility seems to have been ruled out by subsequent discussions [4,5], including no-go theorems for a broad class of systems [6,7].

Surprisingly, it was later shown that systems in the presence of periodic driving, generally described by Floquet theory, can indeed self-organize and present a subharmonic response in the observables [8–10]. The phase which exhibits the features of spatiotemporal order now recognized in time crystals was also classified as the π spin glass [11], and since then a precise definition has been put forward [12]. The properties of these systems have been studied in radically different configurations, such as atoms bouncing off an oscillating mirror [13] or spin chains in the presence of disorder and many-body localization [14]. The latter proved to be an ideal starting point for experiments and resulted in the first two observations of time crystals. While these experiments dealt with two rather distinct arrangements (one exploring nitrogen vacancies in diamonds [15] and the other a chain of trapped ions [16]), both had as a major feature the presence of disorder. Since the external driving in such systems leads to heating and eventual thermalization, it is generally assumed that Floquet time crystals should occur in a prethermal regime. The existence of a many-body localized regime serves, in this context, as a source of stabilization against thermal effects.

Other studies have shown, however, that disorder is not a crucial requirement for the realization of discrete time crystals [17]. Cold atomic systems, for instance, can sustain a time-crystal phase even in a "clean" setup where disorder is absent [18]. Experimentally, time-crystal phases have been observed in ordered spin systems with nuclear magnetic resonance techniques [19,20]. In these studies, the presence of interactions between atoms or spins is the decisive factor leading up to time-translation-symmetry breaking. The manifestation of quasicrystalline order and its transition to a time crystal has been observed with Bose-Einstein condensates under the action of periodically driven magnetic fields [21].

These developments open the interesting possibility of searching for a time-crystal behavior in different platforms, away from the many-body limit and in the absence of disorder. To address this matter, we present a proposal for observing the breaking of discrete time-translation symmetry in few-body systems, which can be realized in two ways (see Fig. 1 for a schematic depiction of each case). The first involves a small ensemble of cold trapped atoms, where the interactions between different components can be tuned by means of Feshbach [22] or confinement-induced resonances [23]. In the limit of strong interactions, the system behaves as a spin chain, where the exchange coefficients are determined by the shape of the trapping potential [24,25]. Periodically driving the system with spin-flip pulses [26] results in a response in the magnetization which depends highly on the choice of interaction parameters. Moreover, we show that realizing the system with fermionic or bosonic atoms—the latter assuming that interactions between identical particles can be tuned—yields very distinct results.

*rafael@phys.au.dk; rafael.barfknecht@ufrgs.br
†stig@phys.au.dk
‡angela@if.ufrgs.br
§zinner@phys.au.dk

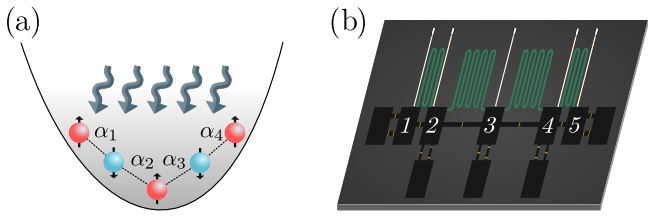

FIG. 1. Schematic depiction of the two few-body systems under consideration: (a) an ensemble of cold atoms in a harmonic trap, where the strong interactions allow for a mapping of the system to a spin chain with position-dependent exchange coefficients, and (b) a superconducting circuit consisting of five superconducting islands, each corresponding to a spin (see Appendix E for a detailed representation of the circuit in a chip). The driving protocol can be realized by applying spin-flip pulses (represented by the gray arrows on the left panel). In the superconducting circuit, the pulses can be introduced as Rabi oscillations acting on each island through the white control lines.

The second realization is based on a circuit consisting of five superconducting islands coupled via Josephson junctions and inductors [27–30]. Superconducting circuits can be used as platforms for simulations in atomic physics and quantum optics [31,32]. Under certain conditions, this system can also be interpreted as a spin chain [33,34]; more importantly, by detuning the frequencies of the spins in our model and employing the rotating wave approximation (RWA), we get a Hamiltonian described only by Ising couplings. By applying an external field to the islands for a short period of time, Rabi oscillations can be induced to each spin, causing them to flip.

II. SYSTEM DESCRIPTION

We consider a general XXZ spin chain described by the following Hamiltonian:

$$H = \sum_{i=1}^{N-1}\left[\eta_i^0 + \sum_{k=x,y,z}\eta_i^k\sigma_i^k\sigma_{i+1}^k\right] - \frac{1}{2}\sum_{i=1}^{N}\Omega_i\sigma_i^z, \qquad (1)$$

where we take a set of inhomogeneous coefficients η_i. The values of these coefficients are determined next, according to the specified model. We also include a site-dependent constant η_i^0 and the possibility of an inhomogeneous external field with frequency Ω_i. Contrary to some theoretical approaches [35,36] and experiments [15], our model does not require long-range interactions. We focus on a system of $N = 5$ spins and our protocol for the external driving is fairly simple: we choose an initial antiferromagnetic state, such as $|\psi(0)\rangle = |\uparrow\downarrow\uparrow\downarrow\uparrow\rangle$, which is not an eigenstate of the spin chain under any nontrivial parameter configuration. We then realize a sequence of spin-flip operations (with period T_D) at each site, rotating all spins by an angle θ. We consider initially an instantaneous rotation, but we extend our results in superconducting circuits to the case of finite-time rotations, which are more realistic from an experimental viewpoint. By keeping track of the time evolution of the magnetization, $m(t) = \langle\psi(t)|\sum_{i=1}^{N}\sigma_i^z|\psi(t)\rangle$, we register the response of the system to the external driving. For perfect ($\theta = \pi$) pulses, the magnetization has a trivial periodicity of $T_m = 2T_D$. However, for imperfect rotations described by $\theta = \pi - \epsilon$, we obtain a different response, which is strongly determined by the presence of interactions between the spins. In the following, we focus on pulse imperfections of a constant value. However, we have also taken into account cases with slightly modulated pulses (see Appendix B) and even situations where the imperfections are randomly determined. While this may affect the outcome in the noninteracting regime, we find that the interacting results still hold.

A. Two-component trapped cold gases

Our first application of the protocol described above is an interacting system of trapped cold atoms. Some proposals for the realization of time crystals with ultracold atoms involve the many-body problem of bosons in the presence of a periodic Hamiltonian [37,38], which is generally described by the Gross-Pitaevskii equation. In the present case, we focus on the few-body problem of bosonic atoms with two internal components, which we label as the pseudospin states $|\uparrow\rangle$ and $|\downarrow\rangle$. We assume contact interactions given by $g\sum_{i<j}\delta(x_i - x_j)$ for atoms in different internal states and $\kappa g\sum_{i<j}\delta(x_i - x_j)$ for atoms in the same internal state. All atoms are confined by an effectively one-dimensional harmonic trap described by $V(x) = \frac{1}{2}m\omega^2x^2$. For simplicity, we assume the atoms to have the same mass $m = 1$, and define the trapping frequency as $\omega = 1$.

In the limit of strong interactions ($g \gg 1$), this system can be described, up to linear order in $1/g$, by an effective spin chain [24,39] (see Appendix A), which can be obtained from Hamiltonian (1). In this description, we make the substitutions $\eta_i^0 = -\frac{1}{2}\frac{\alpha_i}{g}(1 + \frac{2}{\kappa})$, $\eta_i^x = \eta_i^y = \frac{1}{2}\frac{\alpha_i}{g}$, and $\eta_i^z = \frac{1}{2}\frac{\alpha_i}{g}(1 - \frac{2}{\kappa})$, where g and κ have the meaning defined above, and α_i are position-dependent exchange coefficients, which are determined solely by the trapping geometry. These coefficients have been calculated for traps of different shapes and systems of up to $N \approx 30$ [40,41]. Particularly for the case of $N = 5$ in a harmonic trap with trapping frequency $\omega = 1$, we have $\alpha_1 = \alpha_4 \approx 2.16612$ and $\alpha_2 = \alpha_3 \approx 3.17738$, where the symmetry of the coefficients in guaranteed by the parity invariance of the trap. With this mapping (and considering $\Omega_i = 0$), Hamiltonian (1) can now be written as

$$H = -\frac{1}{2}\sum_{i}^{N-1}\frac{\alpha_i}{g}\left[\frac{1}{2}(1 - \vec{\sigma}_i\cdot\vec{\sigma}_{i+1}) + \frac{1}{\kappa}\left(1 + \sigma_i^z\sigma_{i+1}^z\right)\right], \qquad (2)$$

where the magnitude of the term on the right is determined by the value of the intraspecies interaction parameter κ. While this Hamiltonian describes a system of strongly interacting bosons (due to the presence of interactions between identical components), we can reproduce a fermionic system by

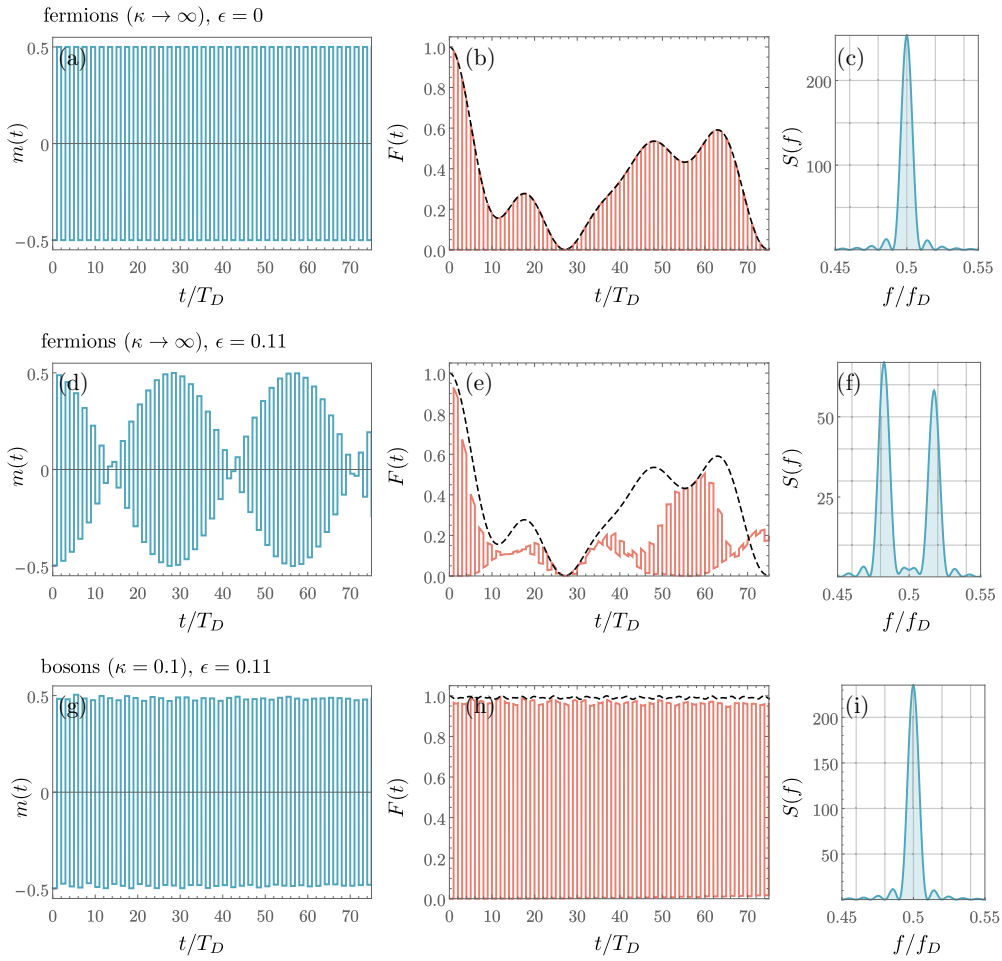

FIG. 2. Time evolution of observables in a system of $N = 5$ harmonically trapped atoms. The parameter κ defines the atomic species (fermionic or bosonic) and the value of ϵ determines the presence of imperfections in the driving (for $\epsilon = 0$ we have a perfect π pulse). (a), (d), (g) Time evolution of the magnetization and (b), (e), (h) the analogous results for the overlap with the initial state $F(t)$. In these figures, the black dashed curves show the results for $F(t)$ in the absence of driving. (c), (f), (i) The spectral density obtained through the Fourier transform of $m(t)$.

taking the limit $\kappa \to \infty$. Then, we obtain $H = -\sum_{i=1}^{N-1} \frac{\alpha_i}{g}(1 - P_{i,i+1})$, where $P_{i,i+1} = \frac{1}{2}(1 + \vec{\sigma}_i \cdot \vec{\sigma}_{i+1})$ is the permutation operator that exchanges neighboring spins. We focus on calculating the time evolution of the magnetization under the periodic action of the spin-flip operator $O = \exp(-i\frac{\theta}{2}\sum_{i=1}^{N}\sigma_i^x)$.

In Figs. 2(a)–2(c) we show, respectively, the results for the time evolution of the magnetization $m(t)$, the overlap probability of the wave function with the initial state $F(t) = |\langle\psi(0)|\psi(t)\rangle|^2$, and the spectral density $S(f) = |\hat{m}(f)|^2$, where $m(f) = \int dt\, e^{-2\pi i f t} m(t)$ is the Fourier transform of the magnetization. We initially assume a periodic pulse that rotates the spins by an angle of $\theta = \pi$ at times $t = nT_D$ with n being an integer. We find that the magnetization oscillates with a period twice as large as the driving, which results in a peak in $f = f_D/2$ where f_D is the driving frequency. While this quantity only registers the global behavior of the system, the overlap with the initial state $F(t)$ describes its underlying spin dynamics. When all spins are rotated by π with respect to the initial state, we have $F(t) = 0$. In the remaining times, we observe that the time evolution of the spin distribution is described by the exact results in the absence of periodic driving (black dashed curves).

If we consider an imperfect pulse with $\theta = \pi - \epsilon$, we observe two different results. In the case of fermions [Figs. 2(d)–2(f)], the magnetization now exhibits a beating pattern that destroys the subharmonic peak at $f = f_D/2$. The overlap $F(t)$ is no longer described by the result in the absence of driving. For bosons [Figs. 2(g)–2(i)], on the other hand, the presence of a dominating interaction between identical spins—defined by the small value of κ—locks back the magnetization response peak at $f = f_D/2$, even for $\epsilon \neq 0$. This robustness of the response to imperfect pulses is one of the essential features of a time-crystal phase [14]. In fact, here we find that it arises under fairly simple conditions, without the need for switching interactions on and off as part of the driving protocol. It is interesting to notice that, for a frame of reference simultaneously rotating with the spin-flip pulses, the magnetization seems to acquire a nearly constant value, an effect than has recently been dubbed "crypto-equilibrium" [42]. Having the

freedom to tune interactions between the atoms presents the possibility of studying the "melting" of time crystals as these parameters are modified. This could be implemented, for instance, by taking a bosonic system and tuning κ from small to large.

While experimental realizations with fermions frequently deal with ^{6}Li atoms [43], two-component bosonic systems can be produced with a gas of ^{87}Rb atoms, where the two lowest hyperfine states are given by $|F = 2, m_f = -1\rangle$ and $|F = 1, m_f = 1\rangle$. Imbalance in the interactions can be introduced, for instance, by means of confinement-induced resonances [44]. The atoms can then be driven between the two different hyperfine states through Raman pulses, with a typical frequency of $\sim$6834 MHz. An important feature of these systems is that the energy and time scales can be controlled by modifying the external confinement (the inverse frequency of the harmonic trap in a few-body experiment is $\sim 100\ \mu$s; see Appendix B for a simulation of the system in a lattice). Recent works with multicomponent bosonic ^{87}Rb systems indicate a lifetime of the order of microseconds with minimal heating originating from Raman processes [45].

The driving protocol employed here can be also used in the case of systems with more than two internal components, as long as Ising-type interactions are dominant in the Hamiltonian. By periodically switching between different pseudospin states, it is possible to expect a fractional response frequency given by $f = f_D/\nu$, where ν is the number of internal states available. Multicomponent cold atomic gases, such as fermionic systems with SU(N) symmetry, have been theoretically explored [46,47] and can be realized in the laboratory [48,49]. A recent proposal for realizing time crystals in SU(N) systems explores the ladder of internal states as a synthetic dimension [18]. In a more extreme example, systems where the response frequency is much smaller than the driving frequency have been obtained in the framework of atoms bouncing off an oscillating mirror [37].

B. Superconducting circuits

As a second implementation, we apply the formalism described above to the case of a superconducting circuit. The circuit consists of five C-shunted flux qubits [50]—which are interesting for experimental realization due to their long decoherence time—but other types of superconducting qubits can be used [51]. The qubits are pairwise connected with Josephson junctions and inductors, and the outer islands are also connected through capacitors (see Appendix C for a lumped circuit sketch). An external driving field is applied to each node in order to drive the rotation of spins.

By applying Devoret's quantum treatment of electromagnetic circuits [52,53], we derive a Hamiltonian which can again be taken as a particular case of Eq. (1) (see Appendix C for details). Due to the anharmonicity of the Josephson junctions, we truncate our description into the two lowest energy levels, which leaves us with an effective spin model. We require a detuning of the spin frequencies and use the RWA to remove all interactions but the Ising couplings $J_i^z \sigma_i^z \sigma_{i+1}^z$, where $J_i^z = \eta_i^z$ in Eq. (1). In order to realize the rotations between internal states we drive the circuit for a short period of time. In our truncated spin model the driving can be described by $H_D = \frac{A}{2} \sum_{i=1}^{N} (Q_i(t)\sigma_i^y - I_i(t)\sigma_i^x)$, where A is the amplitude of the external fields, and I_i and Q_i are the envelopes of the pulses. To create Rabi oscillations between $|\uparrow\rangle$ and $|\downarrow\rangle$, we match the driving and qubit frequencies and make $A \gg J_i^z$. The driving period is thus given by $\Delta t = (\pi - \epsilon)/A$, which, for large A, is a very short time. In order to avoid heating to higher excited states, we employ the gradient ascent pulse engineering (GRAPE) scheme, which allows for tailoring the envelopes of the pulse such that no heating occurs [54–56] (see Appendix D for details). Choosing realistic variables for the circuit, we obtain a set of experimentally achievable parameters for our spin model. In Table I we show the values for the qubit frequencies Ω_i and the exchange coefficients J_i^z in the interacting cases. We consider a symmetric set of frequencies and exchange coefficients, such that $\Omega_5 = \Omega_1$, $\Omega_4 = \Omega_2$ and $J_3^z = J_2^z$, $J_4^z = J_1^z$.

TABLE I. Spin model parameters used in our simulations. For the noninteracting cases, we make $J_i^z = 0$. Due to the symmetry of the system, we have $\Omega_5 = \Omega_1$, $\Omega_4 = \Omega_2$, $J_3^z = J_2^z$, and $J_4^z = J_1^z$.

Site i	1	2	3
$\Omega_i/2\pi$ GHz	11	15	56
$J_i^z/2\pi$ MHz	-58	-48	

We run simulations for the driving described in this section using QUTIP [57], both with and without dephasing and relaxation noise (denoted by ζ), which represents losses and coupling to the environment. The result of these simulations are presented in Fig. 3. The inhomogeneous driving can lead to an interference pattern in the magnetization which is not due to imperfections in the pulse. This interference causes the absolute value of the magnetization, in some cases, to be larger than 0.5 during the driving period. In our simulations we find the interference to be constructive, but destructive patterns are also possible. For imperfect pulses ($\epsilon \neq 0$), we now have two sources of interference acting on the system—the pulse itself and the driving inhomogeneities. This again leads to a splitting of the half-frequency peak, both in the ideal and inhomogeneous cases. However, the addition of a strong Ising coupling fixes both effects at once, without fine tuning of the parameters.

III. CONCLUSIONS

We have presented a proposal for the realization of discrete time-translation-symmetry breaking in few-body spin chains in the presence of external driving, which can be realized in two distinct ways. In the first case, we apply our formalism to a system consisting of strongly interacting harmonically trapped atoms. A time-crystal behavior arises under the action of a periodic spin-flip driving, provided that the intraspecies repulsion is smaller than the remaining interactions. This leads to the possibility of studying time crystallization in bosonic as opposed to fermionic systems, or even the dynamical "melting" of the time crystal as the intraspecies interactions are tuned. Our second realization shows how a similar result can be achieved in a superconducting circuit. In this

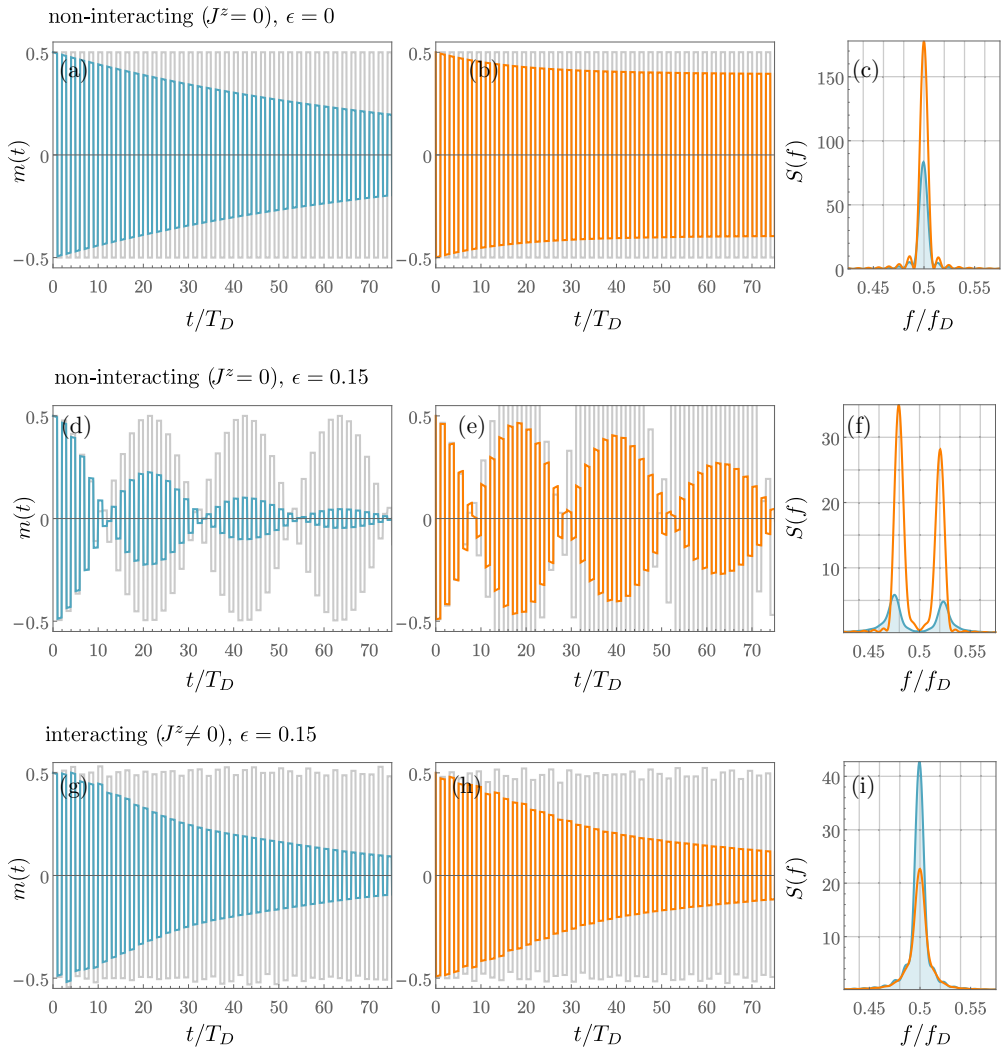

FIG. 3. Time evolution of the magnetization in circuits with (a), (d), (g) ideal driving and (b), (e), (h) inhomogeneous driving. In all plots, the colored curves show the results with an added relaxation noise of $\zeta = 0.05$, while the gray background curves depict the results without losses. The noninteracting cases assume $J_i^z = 0$, while in the interacting cases the parameters are given by Table I. (c), (f), (i) The spectral density of the magnetization, where the colors correspond to the cases of ideal (blue) and inhomogeneous (orange) driving shown on the left.

case, we can introduce the effect of losses and inhomogeneous driving in addition to the imperfection in the pulses. A periodic response which is robust against such imperfections and inhomogeneities is an interesting feature for the implementation of quantum devices based on superconducting circuits [29]. We also present a set of parameters for our quantum system which arises from a realistic circuit model. In neither of the approaches we have to introduce disorder, which is a common feature in previous studies. Naturally, the results described in our study can be generalized to larger chains or systems with more internal degrees of freedom.

In the Appendixes, we provide information on the physical systems considered in our realization of the spin chain and details of experimental possibilities. In Appendix A, we detail the mapping between the Hamiltonian describing an effectively one-dimensional strongly interacting two-component system of atoms to a spin chain. In Appendix B, we explore the situation where this system is placed in a lattice potential, while also making it larger in comparison to the case explored in the main text. We additionally consider the possibility of having spin-flip pulses which are not homogeneous throughout the system.

In Appendix C we detail the derivation of the Hamiltonian for the superconducting circuit, where we start with a simple description of the model in terms of a lumped circuit. By employing the RWA, we show how the model can be reduced to an Ising Hamiltonian in the presence of external driving. To address the issue of heating and how to avoid it in an implementation of these circuits, in Appendix D we describe the GRAPE scheme for the spin-flip pulses and also show results for a simulation where heating occurs. In Appendix E, we provide further details on the implementation of the superconducting circuit and present numerical values for the parameters of the system.

ACKNOWLEDGMENTS

The authors thank O. V. Marchukov and A. G. Volosniev for fruitful discussions on time crystals. The following agencies—Conselho Nacional de Desenvolvimento Científico e Tecnológico (CNPq), Coordenação de Aperfeiçoamento de Pessoal de Nível Superior (CAPES), the Danish Council for Independent Research DFF Natural Sciences, the DFF Sapere Aude program, and the Carlsberg Foundation Distinguished Fellowship program—are gratefully acknowledged for financial support. During the completion of this paper we became aware of a related work by Yu *et al.* [58] which discusses similar ideas in a different context.

APPENDIX A: MAPPING THE STRONGLY INTERACTING SYSTEM TO A SPIN-CHAIN HAMILTONIAN

In this section we show details of the mapping between a strongly interacting two-component system of cold atoms in one dimension and the spin chain described by Eq. (1) of our main text. Different methods have been employed to describe this mapping [24,25,46,59]. In the following, we show the equivalence between the energy functionals of these two models, as described in Ref. [39]. We consider initially a system of two-component bosons in one dimension, where we assume the internal states are described by $|\uparrow\rangle$ and $|\downarrow\rangle$ and the interactions are zero range. The Hamiltonian (already considering $\hbar = m = 1$ and the interaction parameter g in units of $\hbar^2/ml$) is given by

$$H = \sum_{i=1}^{N} H_0(x_i) + g\sum_{i=1}^{N_\uparrow}\sum_{j=1}^{N_\downarrow}\delta(x_{\uparrow i} - x_{\downarrow j}) + \kappa g\sum_{i<i'}^{N_\uparrow}\delta(x_{\uparrow i} - x_{\uparrow i'}) + \kappa g\sum_{j<j'}^{N_\downarrow}\delta(x_{\downarrow j} - x_{\downarrow j'}), \quad \text{(A1)}$$

where $H_0(x) = -\frac{1}{2}\frac{\partial^2}{\partial x^2} + V(x)$ is the single-particle Hamiltonian which applies equally to all atoms. In our main text, the potential term is given by a harmonic trap $V(x) = \frac{1}{2}m\omega^2x^2$. The total number of particles in the system is $N = N_\uparrow + N_\downarrow$. In the limit of infinite interactions ($g \to \infty$), the eigenstates of Hamiltonian (A1) can be described by

$$\Psi = \sum_{k=1}^{L(N_\uparrow,N_\downarrow)} a_k P_k \Phi_0(\{x_{\uparrow i}, x_{\downarrow j}\}), \quad \text{(A2)}$$

where the sum runs over the $L(N_\uparrow, N_\downarrow) = \binom{N_\uparrow + N_\downarrow}{N_\uparrow}$ permutations of the coordinates, and P_k is the permutation operator. The wave function Φ_0 is simply the solution for the model in the limit of infinite interactions (the Tonks-Girardeau gas), with the coordinates ordered as $x_{\uparrow 1} < x_{\uparrow 2} < \cdots < x_{\uparrow N_\uparrow} < x_{\downarrow 1} < \cdots < x_{\downarrow N_\downarrow}$, with $i = 1, \ldots, N_\uparrow$ and $j = 1, \ldots, N_\downarrow$. The action of the permutation operator therefore changes the sector in which Φ_0 is described. For very strong finite interactions, we apply the Hellmann-Feynman theorem and get

$$\frac{\partial E}{\partial g} = \sum_{i=1}^{N_\uparrow}\sum_{j=1}^{N_\downarrow}\langle\Psi|\delta(x_{\uparrow i} - x_{\downarrow j})|\Psi\rangle + \kappa\sum_{i<i'}^{N_\uparrow}\langle\Psi|\delta(x_{\uparrow i} - x_{\uparrow i'})|\Psi\rangle + \kappa\sum_{j<j'}^{N_\downarrow}\langle\Psi|\delta(x_{\downarrow j} - x_{\downarrow j'})|\Psi\rangle, \quad \text{(A3)}$$

where terms containing κ account for the interactions between bosons in the same internal state. It is a requirement of the contact interactions that the following conditions be satisfied:

$$\left(\frac{\partial\Psi}{\partial x_{\uparrow i}} - \frac{\partial\Psi}{\partial x_{\uparrow i'}}\right)\Bigg|_{x_{\uparrow i}-x_{\uparrow i'}=0^-}^{x_{\uparrow i}-x_{\uparrow i'}=0^+} = 2\kappa g\Psi(x_{\uparrow i} = x_{\uparrow i'}), \quad \left(\frac{\partial\Psi}{\partial x_{\downarrow j}} - \frac{\partial\Psi}{\partial x_{\downarrow j'}}\right)\Bigg|_{x_{\downarrow j}-x_{\downarrow j'}=0^-}^{x_{\downarrow j}-x_{\downarrow j'}=0^+} = 2\kappa g\Psi(x_{\downarrow j} = x_{\downarrow j'}), \quad \text{(A4)}$$

for pairs of bosons in the same internal state and

$$\left(\frac{\partial\Psi}{\partial x_{\uparrow i}} - \frac{\partial\Psi}{\partial x_{\downarrow j}}\right)\Bigg|_{x_{\uparrow i}-x_{\downarrow j}=0^-}^{x_{\uparrow i}-x_{\downarrow j}=0^+} = 2g\Psi(x_{\uparrow i} = x_{\downarrow j}), \quad \text{(A5)}$$

for a pair in different internal states. Combining Eqs. (A3)–(A5), we get

$$\frac{\partial E}{\partial g} = \frac{K_{\uparrow\downarrow}}{g^2} + \frac{K_{\uparrow\uparrow}}{\kappa g^2} + \frac{K_{\downarrow\downarrow}}{\kappa g^2}, \quad \text{(A6)}$$

with

$$K_{\uparrow\downarrow} = \frac{\sum_{i=1,j=1}^{N_\uparrow,N_\downarrow}\int dx_{\uparrow 1},\ldots,dx_{\uparrow N_\uparrow}\int dx_{\downarrow 1},\ldots,dx_{\downarrow N_\downarrow}\left|\left(\frac{\partial\Psi}{\partial x_{\uparrow i}} - \frac{\partial\Psi}{\partial x_{\downarrow j}}\right)\right|_-^+\Big|^2\delta(x_{\uparrow i} - x_{\downarrow j})}{4\int dx_{\uparrow 1},\ldots,dx_{\uparrow N_\uparrow}\int dx_{\downarrow 1},\ldots,dx_{\downarrow N_\downarrow}|\Psi|^2},$$

$$K_{\uparrow\uparrow} = \frac{\sum_{i<i'}^{N_\uparrow}\int dx_{\uparrow 1},\ldots,dx_{\uparrow N_\uparrow}\int dx_{\downarrow 1},\ldots,dx_{\downarrow N_\downarrow}\left|\left(\frac{\partial\Psi}{\partial x_{\uparrow i}} - \frac{\partial\Psi}{\partial x_{\uparrow i'}}\right)\right|_-^+\Big|^2\delta(x_{\uparrow i} - x_{\uparrow i'})}{4\int dx_{\uparrow 1},\ldots,dx_{\uparrow N_\uparrow}\int dx_{\downarrow 1},\ldots,dx_{\downarrow N_\downarrow}|\Psi|^2},$$

$$K_{\downarrow\downarrow} = \frac{\sum_{j<j'}^{N_\downarrow}\int dx_{\uparrow 1},\ldots,dx_{\uparrow N_\uparrow}\int dx_{\downarrow 1},\ldots,dx_{\downarrow N_\downarrow}\left|\left(\frac{\partial\Psi}{\partial x_{\downarrow j}} - \frac{\partial\Psi}{\partial x_{\downarrow j'}}\right)\right|_-^+\Big|^2\delta(x_{\downarrow j} - x_{\downarrow j'})}{4\int dx_{\uparrow 1},\ldots,dx_{\uparrow N_\uparrow}\int dx_{\downarrow 1},\ldots,dx_{\downarrow N_\downarrow}|\Psi|^2}.$$

Integrating with respect to g we get an energy functional given by

$$E = E_0 - \left(\frac{K_{\uparrow\downarrow}}{g} + \frac{K_{\uparrow\uparrow}}{\kappa g} + \frac{K_{\downarrow\downarrow}}{\kappa g} \right), \tag{A7}$$

where E_0 is the energy in the impenetrable limit ($g \to \infty$) and we disregard terms of higher order than $1/g$. Plugging the wave function (A2) into this expression, we get

$$E = E_0 - \frac{\sum_{i=1}^{N-1} \frac{\alpha_i}{g} \left(\sum_{k=1}^{L(N_\uparrow - 1, N_\downarrow - 1)} A_{ik}^{\uparrow\downarrow} + \frac{2}{\kappa} \sum_{k=1}^{L(N_\uparrow - 2, N_\downarrow)} A_{ik}^{\uparrow\uparrow} + \frac{2}{\kappa} \sum_{k=1}^{L(N_\uparrow, N_\downarrow - 2)} A_{ik}^{\downarrow\downarrow} \right)}{\sum_{k=1}^{L(N_\uparrow, N_\downarrow)} a_k^2} \tag{A8}$$

with

$$A_{ik}^{\uparrow\downarrow} = (a_{ik}^{\uparrow\downarrow} - a_{ik}^{\downarrow\uparrow})^2, \qquad A_{ik}^{\uparrow\uparrow} = (a_{ik}^{\uparrow\uparrow})^2, \qquad A_{ik}^{\downarrow\downarrow} = (a_{ik}^{\downarrow\downarrow})^2, \tag{A9}$$

where $a_{ik}^{ss'}$ represents the coefficients of Eq. (A2) for terms with neighboring spins s and s' at positions i and $i+1$. Therefore, $\alpha_i a_{ik}^{ss'}/g$ generally describe the energy cost of exchanging two neighboring atoms with certain spin projections. The coefficients α_i, however, do not depend on spin, being written as

$$\alpha_i = \frac{\int_{x_1 < x_2 < \cdots < x_N - 1} dx_1 \cdots dx_{N-1} \left| \frac{\partial \Phi_0(x_1, \ldots, x_i, \ldots, x_N)}{\partial x_N} \right|^2_{x_N = x_i}}{\int_{x_1 < x_2 < \cdots < x_N - 1} dx_1 \cdots dx_N |\Phi_0(x_1, \ldots, x_i, \ldots, x_N)|^2}. \tag{A10}$$

It is enough to calculate these integrals in one particular sector, such as $x_1 < x_2 < \cdots < x_N - 1$, to obtain the exchange coefficients which are directly related to the trapping geometry. We now take a spin Hamiltonian (see main text) for two component bosons given by

$$H_s = E_0 - \sum_{i=1}^{N-1} J_i \left[\frac{1}{2}(1 - \vec{\sigma}^i \cdot \vec{\sigma}^{i+1}) + \frac{1}{\kappa}\left(1 + \sigma_z^i \sigma_z^{i+1}\right) \right]. \tag{A11}$$

A spin state for this Hamiltonian can be written as

$$|\chi\rangle = \sum_{k=1}^{L(N_\uparrow, N_\downarrow)} a_k P_k |\uparrow_1 \cdots \uparrow_{N_\uparrow} \downarrow_1 \cdots \downarrow_{N_\downarrow}\rangle, \tag{A12}$$

where again the sum runs over all permutations of the $N_\uparrow$ and $N_\downarrow$. With the energy for Eq. (A11) as $\langle \chi | H_s | \chi \rangle$, we get

$$\langle \chi | H | \chi \rangle = E_0 - \frac{\sum_{i=1}^{N-1} J_i \left(\sum_{k=1}^{L(N_\uparrow - 1, N_\downarrow - 1)} A_{ik}^{\uparrow\downarrow} + \frac{2}{\kappa} \sum_{k=1}^{L(N_\uparrow - 2, N_\downarrow)} A_{ik}^{\uparrow\uparrow} + \frac{2}{\kappa} \sum_{k=1}^{L(N_\uparrow, N_\downarrow - 2)} A_{ik}^{\downarrow\downarrow} \right)}{\sum_{k=1}^{L(N_\uparrow, N_\downarrow)} a_k^2}, \tag{A13}$$

which is precisely the same energy functional as Eq. (A8). Since we obtain the same eigenvalue problem, we have thus checked the validity of the mapping between Eq. (A1) and Eq. (A11).

APPENDIX B: SIMULATION IN A LATTICE POTENTIAL

In this section we extend the simulations shown in the main text to a lattice potential, which is extensively explored in experiments [60]. We increase our spin-chain description of the strongly interacting system to a mixture consisting of $N_\uparrow = 4$ and $N_\downarrow = 3$ atoms and consider each site of the lattice to be populated by a single atom. The presence of the lattice potential is now encoded in a set of homogeneous exchange coefficients α_i. The magnitude of these coefficients can be manipulated experimentally by changing the lattice depth and by consequence the size of the barrier separating a pair of atoms. Additionally, we consider also the presence of a slightly modulated driving pulse described by $O = \exp\left(-i\frac{\theta}{2}\sum_{i=1}^{N} c_i \sigma_i^x\right)$, where $\theta = \pi - \epsilon$ and ϵ is the pulse imperfection. The modulations are thus given by the coefficients c_i and the initial state is kept as $\psi_0 = |\uparrow\downarrow\uparrow\downarrow\uparrow\downarrow\uparrow\rangle$. In Fig. 4 we show a sketch of the system under consideration.

In Fig. 5 we show the results for the time evolution of the magnetization $m(t)$, the overlap with the initial state $F(t)$, and the Fourier peaks of the magnetization $S(f)$. We focus on the perturbed cases where $\epsilon = 0.1$. The fermionic case ($\kappa \to \infty$) again shows beating due to the imperfect pulses, with the possibility of $m(t) > 0.5$ due to the modulation in the pulse. In the bosonic case with $\kappa = 0.1$ we again find the period locking that characterizes the breaking of time-translation symmetry, even with a modulated external pulse. Moreover, the system presents a complex underlying spin dynamics, which is made evident by the disagreement between the behavior of $F(t)$ in the plots and the predicted results in the absence of driving (black dashed curves).

APPENDIX C: FROM LUMPED CIRCUIT TO SPIN MODEL

In this section we derive the spin model consisting of $N = 5$ qubits on a linear chain, starting from the lumped circuit depicted in Fig. 6.

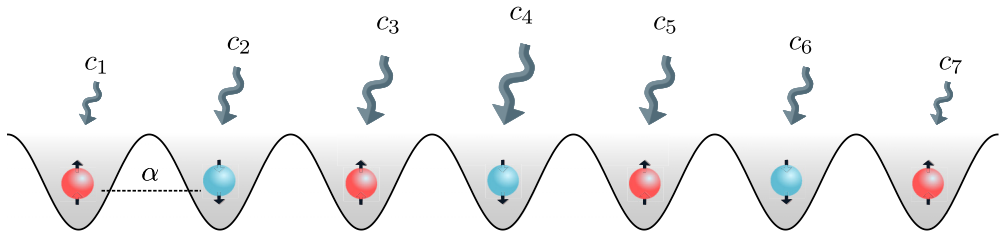

FIG. 4. A system of $N = 7$ atoms in a lattice potential. Our mixture consists of $N_\uparrow = 4$ and $N_\downarrow = 3$ atoms. For simplicity, we assume a set of homogeneous coefficients $\alpha = 1$. The external pulses are represented by the gray arrows and modulated by the coefficients $c_1 = c_7 = 0.98$, $c_2 = c_6 = 0.99$, $c_3 = c_5 = 1.0$, and $c_4 = 1.1$.

Each node of our circuit is marked with a dot and is denoted ϕ_i, $i = 1, \ldots, N$. The lower part of the circuit consists of five C-shunted flux qubits [50] with capacitance $\tilde{C}_i$ and three Josephson junctions. The two junctions in the middle have energy E_i, while the rightmost junction has energy $\alpha_i E_i$, where $\alpha_i \in]0, 0.5[$. Note that even though we simply print a single Josephson junction, it is implicitly assumed that each of these components is a superconducting quantum interference device (SQUID) consisting of two Josephson junctions. The flux through the qubits is given by Φ_i. Note that instead of C-shunted flux qubits one could have used other qubit types, such as transmon [61], X-mon [62], flux [63–65], fluxonium [66], and phase qubits [67].

The nodes are connected by Heisenberg couplers with capacitance $C_{i,i+1}$, inductance $L_{i,i+1}$, and Josephson energy $E_{i,i+1}$. Note that $C_{2,3} = C_{3,4} = 0$. Each node is connected to an external driving field, φ_i, through a capacitor C_i'. We spatially symmetrize the circuit such that $E_i = E_{6-i}$ and likewise for all other components.

Using the quantum treatment of electromagnetic circuits developed by Devoret [52,53] we find the Lagrangian of the system (written in unitless notation)

$$L = 2\sum_{i=1}^{4} C_i \dot{\phi}_i^2 + 2\sum_{i=1}^{3} C_{i,i+1}(\dot{\phi}_i - \dot{\phi}_{i+1})^2 - U(\vec{\phi}) + L_d(\vec{\phi}, \vec{\varphi}), \tag{C1}$$

where we have introduced $C_i = \tilde{C}_i + C_i'$ for convenience. The potential of the system is given by

$$U(\vec{\phi}) = -\sum_{i=1}^{5} E_i \left[2\cos\frac{\phi_i}{2} + \alpha_i \cos(\phi_i + \Phi_i) \right] - \sum_{i=1}^{4} E'_{i,i+1} \cos(\phi_i - \phi_{i+1}) + \frac{1}{2}\sum_{i=1}^{4} \frac{(2\pi)^2}{L_{i,i+1}} (\phi_i - \phi_{i+1})^2, \tag{C2}$$

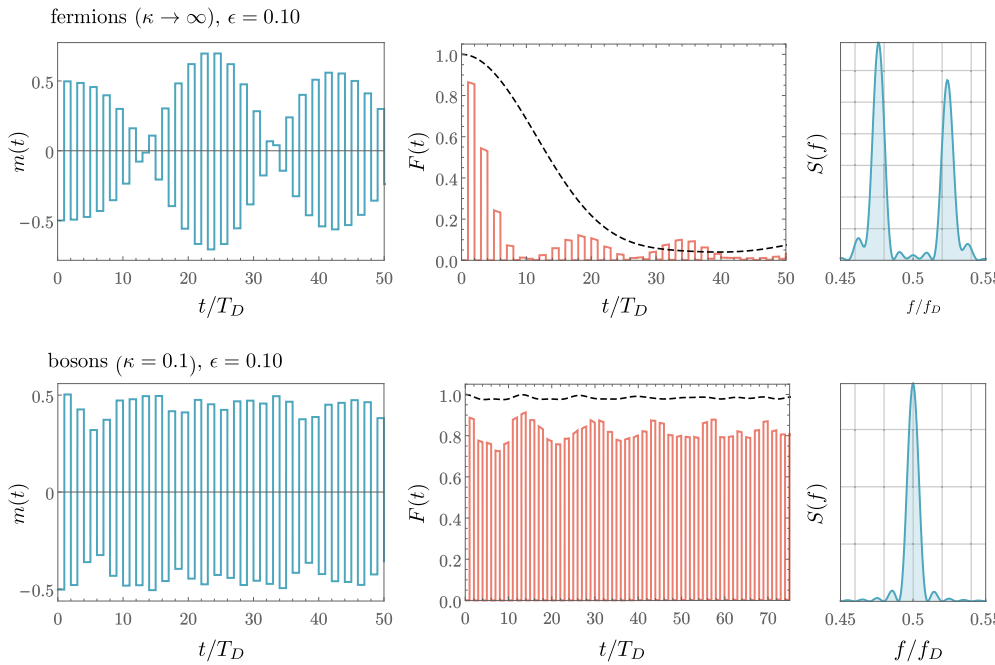

FIG. 5. Time evolution of the magnetization $m(t)$ (left column), the overlap with the initial state $F(t)$ (center column), and the Fourier peaks of the magnetization $S(f)$ (right column). The top panels show the results for fermions, while the bottom panels correspond to bosons. The black dashed curves show the results for $F(t)$ in the absence of external driving. The driving period and driving frequency are denoted by T_D and f_D, respectively.

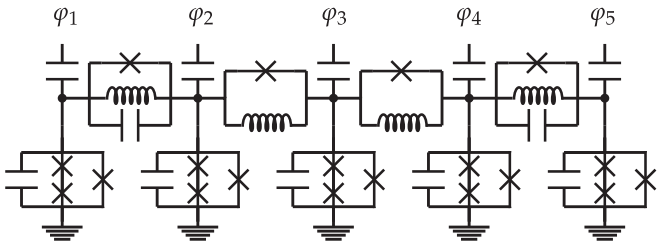

FIG. 6. Diagram for the circuit used to implement a linear Heisenberg spin chain with five qubits. The dots mark the circuit nodes and the x's mark Josephson junctions, while the capacitor, inductors, and ground are denoted with the usual symbols. See the main text for the naming of the elements.

while the external driving yields

$$L_d(\vec{\phi},\vec{\varphi}) = \frac{1}{2}\sum_{i=1}^{5} C_i'(\dot{\phi}_i - \dot{\varphi}_i(t))^2. \tag{C3}$$

Changing to the Hamiltonian formalism and quantizing the system, we arrive at the Hamiltonian described by

$$H = 4\vec{p}^T\mathcal{K}^{-1}\vec{p} + U(\phi) + H_D, \tag{C4}$$

where $\vec{p}$ is the vector of generalized momentum and $\mathcal{K}$ is the capacitance matrix given by

$$K = 8\begin{pmatrix} C_1 + C_{1,2} & -C_{1,2} & 0 & 0 & 0 \\ -C_{1,2} & C_2 + C_{1,2} & 0 & 0 & 0 \\ 0 & 0 & C_3 & 0 & 0 \\ 0 & 0 & 0 & C_4 + C_{4,5} & -C_{4,5} \\ 0 & 0 & 0 & -C_{4,5} & C_5 + C_{4,5} \end{pmatrix}. \tag{C5}$$

Since this matrix is block diagonal, its inverse will also be block diagonal, meaning that we avoid crosstalk in the circuit. Here, we include the external driving in the Hamiltonian as H_D, which we come back to later.

We now focus on the potential and parametrize the external fluxes as

$$\Phi_i = \pi - 2\pi f_i, \tag{C6}$$

where f_i must be in the range $[-0.5, 0.5]$. This changes the potential into

$$U(\vec{\phi}) = -\sum_{i=1}^{5} E_i\left[2\cos\frac{\phi_i}{2} - \alpha_i\cos(\phi_i - 2\pi f_i)\right] - \sum_{i=1}^{4} E'_{i,i+1}\cos(\phi_i - \phi_{i+1}) + \frac{1}{2}\sum_{i=1}^{4}\frac{(2\pi)^2}{L_{i,i+1}}(\phi_i - \phi_{i+1})^2. \tag{C7}$$

By expanding this potential around its minimum [which we denote as $\vec{\phi}^0 = (\phi_1^0, \phi_2^0, \phi_3^0, \phi_4^0)$], we obtain

$$\begin{aligned} U(\vec{\phi}) \simeq & \sum_{i=1}^{5}\frac{E_i}{2}\left[\frac{1}{2}\cos\frac{\phi_i^0}{2} - \alpha_i\cos\left(\phi_i^0 - 2\pi f_i\right)\right]\left(\phi_i - \phi_i^0\right)^2 - \sum_{i=1}^{5}\frac{E_i}{24}\left[\frac{1}{8}\cos\frac{\phi^0}{2} - \alpha_i\cos\left(\phi_i^0 - 2\pi f_i\right)\right]\left(\phi_i - \phi_i^0\right)^4 \\ & + \sum_{i=1}^{4}\left[\frac{E_{i,i+1}}{2}\left(\phi_i - \phi_{i+1} - \phi_{i,i+1}^0\right)^2 - \frac{E_{i,i+1}}{24}\left(\phi_i - \phi_{i+1} - \phi_{i,i+1}^0\right)^4\right] + \sum_{i=1}^{4}\frac{(2\pi)^2}{2L_{i,i+1}}(\phi_i - \phi_{i+1})^2, \end{aligned} \tag{C8}$$

where all irrelevant constant terms have been removed, and we have defined $\phi_{i,i+1}^0 = \phi_i^0 - \phi_{i+1}^0$. Expanding the parentheses and once again removing all constant terms yields

$$\begin{aligned} U(\vec{\phi}) = & \sum_{i=1}^{5}\frac{E_i}{2}\left[\frac{1}{2}\cos\frac{\phi_i^0}{2} - \alpha_i\cos\left(\phi_i^0 - 2\pi f_i\right)\right]\left(\phi_i^2 - 2\phi_i\phi_i^0\right) - \sum_{i=1}^{5}\frac{E_i}{24}\left[\frac{1}{8}\cos\frac{\phi_i^0}{2} - \alpha_i\cos\left(\phi_i^0 - 2\pi f_i\right)\right] \\ & \times\left(\phi_i^4 - 4\phi_i^3\phi_i^0 + 6\phi_i^2\left(\phi_i^0\right)^2 - 4\phi_i\left(\phi_i^0\right)^3\right) + \sum_{i=1}^{4}\frac{E_{i,i+1}}{2}\left(\phi_i^2 + \phi_{i,i+1}^2 - 2\phi_i\phi_{i,i+1} + 2\phi_{i,i+1}^0(\phi_{i,i+1} - \phi_i)\right) \\ & - \sum_{i=1}^{4}\frac{E_{i,i+1}}{24}\left(\phi_i^4 + \phi_{i,i+1}^4 - 4\phi_i^3\phi_{i,i+1} + 6\phi_i^2\phi_{i,i+1}^2 - 4\phi_i\phi_{i,i+1}^3 - 4\phi_i^3\phi_{i,i+1}^0\right. \\ & + 12\phi_i^2\phi_{i,i+1}\phi_{i,i+1}^0 + 6\phi_i^2\left(\phi_{i,i+1}^0\right)^2 - 12\phi_i\phi_{i,i+1}^2\phi_{i,i+1}^0 - 12\phi_i\phi_{i,i+1}\left(\phi_{i,i+1}^0\right)^2 - 4\phi\left(\phi_{i,i+1}^0\right)^3 + 4\phi_{i,i+1}^3\phi_{i,i+1}^0 \\ & \left. + 6\phi_{i,i+1}^2(\phi_{i,i+1}^0)^2 + 4\phi_{i,i+1}\left(\phi_{i,i+1}^0\right)^3\right) + \sum_{i=1}^{4}\frac{(2\pi)^2}{2L_{i,i+1}}\left(\phi_i^2 + \phi_{i,i+1}^2 - 2\phi_i\phi_{i,i+1}\right). \end{aligned}$$

Since we wish to employ the RWA, we can now remove all terms with an odd power of the node fluxes. The potential thus reduces to

$$U(\vec{\phi}) = \sum_{i=1}^{5} \frac{E_i}{2}\left[\frac{1}{2}\cos\frac{\phi_i^0}{2} - \alpha_i \cos\left(\phi_i^0 - 2\pi f_i\right)\right]\phi_i^2 - \sum_{i=1}^{5} \frac{E_i}{24}\left[\frac{1}{8}\cos\frac{\phi_i^0}{2} - \alpha_i \cos\left(\phi_i^0 - 2\pi f_i\right)\right]\left(\phi_i^4 + 6\phi_i^2\left(\phi_i^0\right)^2\right)$$
$$+ \sum_{i=1}^{4} \frac{E_{i,i+1}}{2}\left(\phi_i^2 + \phi_{i,i+1}^2 - 2\phi_i\phi_{i,i+1}\right) - \sum_{i=1}^{4} \frac{E_{i,i+1}}{24}\left(\phi_i^4 + \phi_{i,i+1}^4 - 4\phi_i^3\phi_{i,i+1} + 6\phi_i^2\phi_{i,i+1}^2 - 4\phi_i\phi_{i,i+1}^3\right.$$
$$\left. + 6\phi_i^2\left(\phi_{i,i+1}^0\right)^2 - 12\phi_i\phi_{i,i+1}\left(\phi_{i,i+1}^0\right)^2 + 6\phi_{i,i+1}^2\left(\phi_{i,i+1}^0\right)^2\right) + \sum_{i=1}^{4} \frac{(2\pi)^2}{2L_{i,i+1}}\left(\phi_i^2 + \phi_{i,i+1}^2 - 2\phi_i\phi_{i,i+1}\right).$$

We are now in a position to collect terms. This yields the full Hamiltonian

$$H = \sum_{i=1}^{5}\left[4E_{C,i}\hat{p}_i^2 + \frac{1}{2}(E_{L,i} + E_{J,i})\phi_i^2 - \frac{E_{J,i}}{24}\phi_i^4\right] + \sum_{i=1}^{4}\left[F_{i,i+1}^{XX}\phi_i\phi_{i+1} + G_{i,i+1}^{XX}\left(\phi_i^3\phi_{i+1} + \phi_i\phi_{i+1}^3\right)\right.$$
$$\left. + F_{i,i+1}^{ZZ}\phi_i^2\phi_{i+1}^2\right] + 8(\mathcal{K}^{-1})_{(1,2)}(\hat{p}_1\hat{p}_2 + \hat{p}_4\hat{p}_5) + \hat{H}_D, \tag{C9}$$

where the effective energies of the capacitor $E_{C,i}$ are given by the diagonal elements of the inverse capacitance matrix. The effective energies of the Josephson junctions are given by

$$E_{J,i} = E_i\left[\frac{1}{8}\cos\frac{\phi_i^0}{2} - \alpha_i\cos\left(\phi_i^0 - 2\pi f_i\right)\right] + E_{i-1,i} + E_{i,i+1}, \tag{C10}$$

where $E_{0,1} = E_{5,6} = 0$. Similarly, the effective energies of the inductors are

$$E_{L,i} = \frac{3E_i}{8}\cos\frac{\phi_i^0}{2} - \frac{E_i}{2}\left[\frac{1}{8}\cos\frac{\phi_i^0}{2} - \alpha_i\cos\left(\phi_i^0 - 2\pi f_i\right)\right]\left(\phi_i^0\right)^2 - \frac{E_{i-1,i}}{2}\left(\phi_{i-1,i}^0\right)^2 - \frac{E_{i,i+1}}{2}\left(\phi_{i,i+1}^0\right)^2 + \frac{(2\pi)^2}{L_{i-1,i}} + \frac{(2\pi)^2}{L_{i,i+1}}, \tag{C11}$$

where again $1/L_{0,1} = 1/L_{5,6} = 0$. The coupling coefficients are given by

$$F_{i,i+1}^{XX} = E_{i,i+1}\left(\frac{1}{2}\left(\phi_{i,i+1}^0\right)^2 - 1\right) - \frac{1}{L_{i,i+1}}, \tag{C12}$$
$$G_{i,i+1}^{XX} = \frac{E_{i,i+1}}{6}, \tag{C13}$$
$$F_{i,i+1}^{ZZ} = -\frac{E_{i,i+1}}{4}. \tag{C14}$$

Changing into ladder operators, we obtain

$$H = \sum_{i=1}^{5}[S_i b_i^\dagger b_i - E_{J,i}T_i^4(b_i^\dagger + b_i)^4] + 2(\mathcal{K}^{-1})_{(1,2)}(T_2T_3)^{-1}(b_2^\dagger - b_2)(b_3^\dagger - b_3)$$
$$+ \sum_{i=1}^{4}\left[F_{i,i+1}^{XX}T_iT_{i+1}(b_i^\dagger + b_i)(b_{i+1}^\dagger + b_{i+1}) + F_{i,i+1}^{ZZ}T_i^2T_{i+1}^2(b_i^\dagger + b_i)^2(b_{i+1}^\dagger + b_{i+1})^2\right.$$
$$\left. + G_{i,i+1}^{XX}\left\{T_i^3T_{i+1}(b_i^\dagger + b_i)^3(b_{i+1}^\dagger + b_{i+1}) + T_iT_{i+1}^3(b_i^\dagger + b_i)(b_{i+1}^\dagger + b_{i+1})^3\right\}\right] + H_D, \tag{C15}$$

where we have defined

$$S_i = 4\sqrt{\frac{1}{2}E_{C,i}\left(E_{L,i} + E_{J,i}\right)}, \tag{C16}$$
$$T_i = \left(\frac{2E_{C,i}}{E_{L,i} + E_{J,i}}\right)^{1/4}. \tag{C17}$$

We are now ready to truncate the Hamiltonian in Eq. (C15) into a spin model. We write

$$H = -\frac{1}{2}\sum_{i=1}^{5}\Omega_i\sigma_i^z + 2J_1^y\left(\sigma_1^y\sigma_2^y + \sigma_4^y\sigma_5^y\right)$$
$$+ \sum_{i=1}^{4}\left[2J_i^x\sigma_i^x\sigma_{i+1}^x + J_i^z\sigma_i^z\sigma_{i+1}^z\right] + H_D, \tag{C18}$$

where the qubit frequencies are given by

$$\Omega_i = S_i - \tfrac{1}{2}E_{J,i}T_i^4 + 4F^{ZZ}_{i-1,i}T_{i-1}^2T_i^2 + 4F^{ZZ}_{i,i+1}T_i^2T_{i+1}^2, \tag{C19a}$$

and $T_0 = T_6 = 0$. The coupling constants are defined as

$$J_i^x = \tfrac{1}{2}F^{XX}_{i,i+1}T_iT_{i+1} + \tfrac{3}{2}G^{XX}_{i,i+1}\{T_i^3T_{i+1} + T_iT_{i+1}^3\}, \tag{C19b}$$

$$J_i^z = F^{ZZ}_{i,i+1}T_i^2T_{i+1}^2, \tag{C19c}$$

$$J_i^y = -(\mathcal{K}^{-1})_{(i,i+1)}(T_iT_{i+1})^{-1}. \tag{C19d}$$

Notice that Hamiltonian (C18) (with the exception of the external driving) can be directly related to Eq. (1) of the main text, by assuming $\eta_1^y = \eta_4^y = 2J_1^y$, $\eta_2^y = \eta_3^y = 0$, $\eta_i^x = 2J_i^x$, and $\eta_i^z = J_i^z$.

If we had truncated to the three lowest states of the anharmonic oscillator, we find that the energy difference between the first and second excited states is given as

$$\Omega_i' = \Omega - \tfrac{1}{2}E_{J,i}T_i^4. \tag{C20}$$

Thus, the absolute and relative anharmonicities become

$$\Delta_i = \Omega_i' - \Omega_i = -\tfrac{1}{2}E_{J,i}T_i^4, \quad \Delta_i^r = -\tfrac{1}{2}\frac{E_{J,i}T_i^4}{\Omega_i}. \tag{C21}$$

We are in a position to transform into the interaction picture. We choose the noninteracting part of the Hamiltonian as the first sum and by requiring the detuning of all the qubit frequencies (such that $|\Omega_i \pm \Omega_j|$ becomes large for all relevant combination of i and j) the RWA removes all XX and YY couplings. We arrive at

$$H_I = \sum_{i=1}^{4} J^z_{i,i+1}\sigma_i^z\sigma_{i+1}^z + (H_D)_I. \tag{C22}$$

This leaves us just the driving part of the Hamiltonian. Starting from the driving Lagrangian in Eq. (C3) we assume that the external field is given by

$$\begin{aligned}\varphi_i(t) &= \tilde{A}_i s_i(t)\sin(\omega_i t + \theta_i)\\ &= \tilde{A}_i s_i(t)(\cos(\theta_i)\sin(\omega_i t) + \sin(\theta_i)\cos(\omega_i t))\\ &= \tilde{A}_i s_i(t)(I_i\sin(\omega_i t) + Q_i\cos(\omega_i t)),\end{aligned} \tag{C23}$$

where ω_i is the driving frequency, θ_i is the phase, $\tilde{A}_i$ is the amplitude, and $s(t)$ is some envelope wave function. We have further adopted the definitions $I_i = \cos\theta_i$ for the in-phase component and $Q_i = \sin\theta_i$ for the out-of-phase component. Expanding the parentheses, we obtain

$$L_d(\vec{\phi},\vec{\varphi}) = \frac{1}{2}\sum_{i=1}^{5} C_i'\big(\dot{\phi}_i^2 + \dot{\varphi}_i^2(t) - 2\dot{\phi}_i\dot{\varphi}_i(t)\big). \tag{C24}$$

The first term has in fact already been included in the capacitance matrix, and the second is an irrelevant constant term (not in time, but with regards to the coordinates), so we must deal only with the driving terms. Those merely affect the kinetic part of the Hamiltonian, resulting in an offset in the conjugate momentum. After some algebra, the driving term takes the form

$$H_D = -8\sum_{i=1}^{5}\dot{\varphi}_i(t)\sum_{j=1}^{5}(\mathcal{K})^{-1}_{(j,i)}p_i, \tag{C25}$$

and truncating into a spin model we find

$$H_D = -\frac{1}{2}\sum_{i=1}^{5} A_i s_i(t)[I_i\sin(\omega_i t) + Q_i\cos(\omega_i t)]\sigma_i^y, \tag{C26}$$

where we have defined

$$A_i = 8\tilde{A}_i\omega_i\sum_{j=1}^{5}(\mathcal{K})^{-1}_{(j,i)}T_i^{-1}. \tag{C27}$$

By varying $\tilde{A}_i$ we can make sure that $A_i = A$; changing into the interaction picture the driving Hamiltonian becomes

$$\begin{aligned}(H_D)_I &= \frac{iA}{2}\sum_{i=1}^{5} s_i(t)[I_i\sin(\omega_i t) + Q_i\cos(\omega_i t)]\\ &\quad\times\left[\sigma_i^- e^{-i\Omega_i t} - \sigma_i^+ e^{i\omega_i t}\right]\\ &= A\sum_{i=1}^{5} s_i(t)[I_i\sin(\omega_i t) + Q_i\cos(\omega_i t)]\\ &\quad\times\left[\sigma_i^y\cos(\Omega_i t) - \sigma_i^x\sin(\Omega_i t)\right]\\ &= \frac{A}{2}\sum_{i=1}^{5} s_i(t)\big[I_i\big(\sin(\delta_i t)\sigma_i^y - \cos(\delta_i t)\sigma_i^x\big)\\ &\quad + Q_i\big(\cos(\delta_i t)\sigma_i^y - \sin(\delta_i t)\sigma_i^x\big)\big],\end{aligned} \tag{C28}$$

where we have introduced the parameter $\delta_i = \omega_i - \Omega_i$ and we have thrown away all fast rotating terms, i.e., terms with $\omega_i + \Omega_i$. Now we are interested in driving between states very rapidly. Therefore, we must choose $A_i \gg J_i^z$ to ensure that the driving is fast compared to the time scale of the system. This means that we can treat each qubit independently during the Rabi pulses, and hence the energy difference between the two states of a qubit becomes equal to the qubit frequency. In order for the Rabi oscillation to take effect, we must therefore require that $\omega_i = \Omega_i$, and thus the driving term becomes

$$(H_D)_I = \frac{A}{2}\sum_{i=1}^{5} s_i(t)\big[-I_i\sigma_i^x + Q_i\sigma_i^y\big], \tag{C29}$$

and using the definition in Eq. (C23) we see that an in-phase pulse, $\theta = 0$, creates a rotation around the x axis, while an out-of-phase pulse, $\theta = \pi/2$, creates a rotation around the y axis.

The envelope function $s_i(t)$ can, in principle, have an arbitrary shape. To model an instantaneous pulse flip the envelope must be very narrow. However, a narrow envelope pulse combined with a small anharmonicity increases the risk of leakage to higher excited states [68,69]. In order to avoid this we employ the GRAPE driving scheme [54–56]. How to employ this to determine the shape and duration of the pulse is explained in Appendix D.

We obtain the following Hamiltonian for our superconducting circuit truncated to the lowest two

levels:

$$H_I(t) = \begin{cases} \sum_i^{N-1} J_i^z \sigma_i^z \sigma_{i+1}^z + (H_D)_I(t), & nT_1 \leqslant t < nT_1 + \Delta t \\ \sum_i^{N-1} J_i^z \sigma_i^z \sigma_{i+1}^z, & nT_1 + \Delta t \leqslant t < (n+1)T_1, \end{cases} \tag{C30}$$

where naturally we have to choose $T_1 > \Delta t$, and the period becomes $T = 2T_1$. When Δt is small (i.e., when A is large) and the driving frequency matches the qubit frequency ($\omega_i = \Omega_i$), our interacting Hamiltonian presents the required features for the occurrence of time-crystal behavior.

APPENDIX D: GRAPE DRIVING SCHEME

While instantaneous spin-flip pulses are convenient from the point of view of the simulations, they are not realistic in a superconducting circuit setup. Therefore, we need to take into account a finite duration for the pulses. However, if we simply flip each qubit using a pulse with a duration comparable to the time scale of the Ising interaction, then the time-crystal signature characterized by a single Fourier peak is destroyed. This is due to an interference of the Ising coupling with the pulse. Thus, we need to apply a pulse to the qubits with a duration shorter than the time scale of the Ising interaction, such that it is effectively turned off. Creating such a quick pulse means we must consider larger amplitudes, which increases the risk of heating the system (i.e., exciting the qubits to states beyond the two lowest levels). In order to investigate the occurrence of heating, we truncate the Hamiltonian in Eq. (C15) to the three lowest energy states. After the rotating wave approximation the Hamiltonian without the drive now takes the form

$$H_I = -\sum_{i=1}^{N} \Delta_i |2\rangle\langle 2|_i + \sum_{i}^{N-1} J_i^z \sigma_i^z \sigma_{i+1}^z, \tag{D1}$$

where $|2\rangle\langle 2|$ is the second excited state of the ith qubit, and $\sigma_i^z = |0\rangle\langle 0|_i - |1\rangle\langle 1|_i - 3|2\rangle\langle 2|_i$. The driving term takes the form

$$(H_D)_I = A \sum_{i=1}^{5} \big[-I_i(t)\big(\sigma_i^x(0,1) + \sigma_i^x(1,2)\big) + Q_i(t)\big(\sigma_i^y(0,1) + \sigma_i^y(1,2)\big)\big], \tag{D2}$$

where $\sigma_j^x(k,l) = |k\rangle\langle l|_j + |l\rangle\langle k|_j$ and $\sigma_j^y(k,l) = i|l\rangle\langle k|_j - i|k\rangle\langle l|_j$, and we have included the envelope in the coefficients $I_i(t)$ and $Q_i(t)$. Unless the anharmonicity is large (of the order of Ω_i), a simple Gaussian (or similar) driving would reach the second excited states as well as the first excited state. In general, our superconducting circuit yields considerable anharmonicities, which means that heating is bound to happen. In order to avoid this, we employ the GRAPE driving scheme [54–56]. The essence of this scheme is to find a pulse that does not induce heating, but still creates the desired effect on the qubits. In our case we want the time-evolution operator to be equal to a NOT gate (up to a phase), i.e.,

$$U_F = e^{i\theta_1}\big(e^{i\theta_2}|2\rangle\langle 2| + \sigma_i^x(0,1)\big). \tag{D3}$$

We then consider the time evolution of our driving Hamiltonian of the ith Hamiltonian

$$U_i(t) = e^{-i\int_0^t H[I_i(t'),Q_I(t')]dt'/\hbar}, \tag{D4}$$

where we can control I_i and Q_i. We apply the gradient ascent algorithm to

$$\phi_2 = \tfrac{1}{4}[|\langle 0|U_F^\dagger U(\Delta t)|0\rangle + \langle 1|U_F^\dagger U(t_g)|1\rangle|^2], \tag{D5}$$

where Δt is the desired gate time (i.e., the duration of a flip). In order to optimize this process, we introduce the approximation $U_i(\Delta t) = U_i^{(N)} U_i^{(N-1)} \cdots s U_i^{(1)}$, where we have sliced the time interval $[0, \Delta t]$ into N pieces of length δt. In each interval the control and therefore the Hamiltonian is assumed to be constant. Thus, the integral of Eq. (D4) is replaced by a sum, and the propagator of each time step can be written as

$$U_i^{(j)} = e^{-i\delta t H(I_i^{(j)}, Q_i^{(j)})/\hbar}. \tag{D6}$$

With this, the gradient of Eq. (D5) can be easily calculated.

The GRAPE scheme allows for high-fidelity flips of the qubits, thus suppressing all heating to higher levels while using just a few quadratures. As an example, in Fig. 7 we show simulations performed with this scheme for a circuit with five qubits. We have simulated the system with the parameters found in Appendix E and an error of 10% on the pulses. The top row indicates the simulation done for

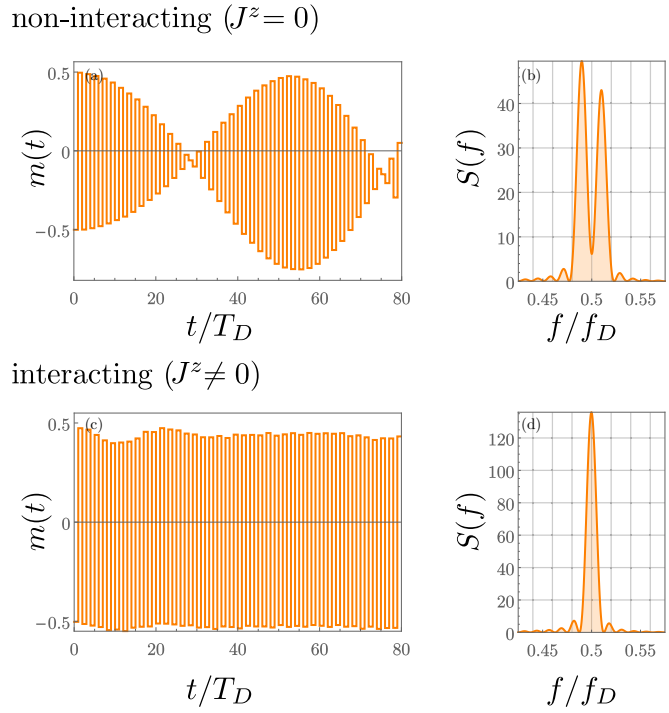

FIG. 7. The Hamiltonian in Eq. (D1) simulated in QUTIP. The first column displays the magnetization of the system, while the second column shows the Fourier transforms. Both cases are with an error of 10% on the pulses, while the first case, (a) and (b), is for $J^z = 0$ and the second case, (c) and (d), is for the J^z's displayed in Table II, where all other parameters have been taken from as well.

no Ising coupling, while the lower row displays the result when the coupling is turned on. The pulse had a duration of 0.5 ns and was not tailored to accommodate the Ising coupling. As in the two-level case discussed in the main text, we observe a beating pattern when there is no Ising coupling, while the time-crystal structure is observed when the Ising coupling is turned on. These structures are further confirmed by the Fourier transform, as seen in the right-hand column. We note that in Fig. 7(a) the beating pattern is slightly tilted downwards, which is due to a small amount of excitations to the third level. This is also the case for the small dip at around $t = 5T$ in Fig. 8(c). However, here the Ising coupling restores the structure after ten periods.

There are several ways to avoid heating in an experimental setup. A longer flip time, t_g, decreases the risk of heating but increases the influence of the Ising coupling. We find that a flip done on the nanosecond scale is sufficient for the time-crystal structure to remain intact. Such a short pulse does limit the amount of possible quadratures in the GRAPE pulse. However, we find that as few as four quadratures are sufficient to create the desired spin-slip effect without heating. This is consistent with current state-of-the-art experimental setups. If such fast pulses are not possible in a given experimental setup, it is also possible to tailor the driving so that the rotations are applied to the entire system rather than to the individual qubits. This means that the pulse will take the Ising interaction into account, and its influence will diminish, allowing for a longer pulse.

APPENDIX E: EXPERIMENTALLY REALISTIC IMPLEMENTATION

Having developed the formalism describing our superconducting circuit, the next question is how to implement such a system with experimentally realistic parameters. First of all we need to go from the lumped circuit diagram in Fig. 6 to a chip. A design possibility is shown in Fig. 8. The chip consists of five superconducting islands numbered from 1 to 5. Connected to each island we have LC resonators, shown in blue. Note that these are not in the lumped circuit model.

A realistic implementation also requires a set of values to be assigned to each element of the circuit. In that respect, a number of conditions must be met:

(1) We would like the qubit frequencies to be pairwise detuned, i.e., $|\Omega_i \pm \Omega_{i+1}| \gg |J_i^x|$. Here it is important that the detuning is much larger than the XX coupling, since we want to "rotate" this coupling away. Usually, we expect the coupling constants to be on the order of 10–300 MHz, while the qubit frequencies usually lie in the gigahertz range.

(2) The C-shunted flux qubit functions best when the effective energies obey the following requirements: $E_{j,i}/E_{C,i} \gtrsim 50$ and $E_{L,i} \sim E_{J,i}$. We further require the anharmonicity of the third energy level to be at least 1% of the energy difference between the two lowest states.

(3) The circuit parameters must fall within the range of values which are experimentally accessible. Capacitors must lie in the range [1,100] fF, while inductors usually lie in the range [0.1,20] nH. Josephson junctions fall in the range $[10, 200]2\pi$ GHz; however, by exploiting the SQUIDs we can expand the range to $[-400, 400]2\pi$ GHz. The C-shunted flux qubit works best when the α-coefficient is in the range [0,0.5] [50].

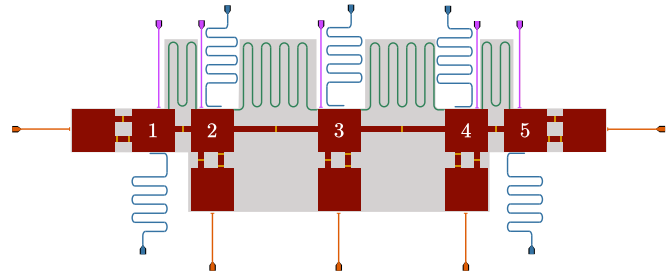

FIG. 8. Sketch of a possible physical chip design of the proposed circuit in Fig. 6. Each numbered box is a superconducting island corresponding to a node. Josephson junctions are shown as narrow yellow strips. Bent wires are inductors. The gray area indicates nongrounded. The orange lines are flux lines, while the purple lines are control and driving of the qubits. The blue wires are resonators used for readout.

The circuit is thus characterized by 17 parameters, which results in a vast parameter space. Therefore, we construct a cost function which returns small values when the above requirements are met or larger values when they are not. This issue is thus reduced to a minimization problem, which can be solved in a variety of ways. We exploited a Nelder-Mead simplex method with randomized initial conditions. Since we have rather few requirements compared to the size of the parameter space, there are several solutions to this minimization problem. We present one such solution in Table II. Table II(a) displays the circuit parameters, while Table II(b) shows the resulting effective energy ratios and spin model parameters.

TABLE II. Circuit parameters and corresponding spin model parameters considered in the main text.

(a) Circuit parameters

i	1	2	3
$E_i/2\pi$ GHz	263.11	−252.84	61.33
$E_{i,i+1}/2\pi$ GHz	56.40	30.60	
C_i/fF	87.37	67.56	13.51
$C_{i,i+1}$/fF	17.41		
$L_{i,i+1}$/nH	8.72	12.65	
α_i	0.314	0.073	0.237
f_i	−0.367	0.317	0.442

(b) Effective ratios and spin model parameters

i	1	2	3
$E_{J,i}/E_{C,i}$	334	389	56
$E_{L,i}/E_{J,i}$	0.32	0.37	2.34
$\Omega_i/2\pi$ GHz	11	15	55
$\Delta_i/2\pi$ MHz	–144	–173	–430
Δ_i^r	−1.3%	−1.6%	−3.9%
$J^x_{i,i+1}/2\pi$ MHz	–311	159	
$J^z_{i,i+1}/2\pi$ MHz	–58	–48	

[1] F. Wilczek, Quantum Time Crystals, Phys. Rev. Lett. **109**, 160401 (2012).

[2] A. Shapere and F. Wilczek, Classical Time Crystals, Phys. Rev. Lett. **109**, 160402 (2012).

[3] T. Li, Z.-X. Gong, Z.-Q. Yin, H. T. Quan, X. Yin, P. Zhang, L.-M. Duan, and X. Zhang, Space-Time Crystals of Trapped Ions, Phys. Rev. Lett. **109**, 163001 (2012).

[4] P. Bruno, Comment on "Space-Time Crystals of Trapped Ions", Phys. Rev. Lett. **111**, 029301 (2013).

[5] P. Bruno, Comment on "Quantum Time Crystals", Phys. Rev. Lett. **110**, 118901 (2013).

[6] P. Bruno, Impossibility of Spontaneously Rotating Time Crystals: A No-Go Theorem, Phys. Rev. Lett. **111**, 070402 (2013).

[7] H. Watanabe and M. Oshikawa, Absence of Quantum Time Crystals, Phys. Rev. Lett. **114**, 251603 (2015).

[8] V. Khemani, A. Lazarides, R. Moessner, and S. L. Sondhi, Phase Structure of Driven Quantum Systems, Phys. Rev. Lett. **116**, 250401 (2016).

[9] D. V. Else, B. Bauer, and C. Nayak, Floquet Time Crystals, Phys. Rev. Lett. **117**, 090402 (2016).

[10] K. Sacha and J. Zakrzewski, Time crystals: A review, Rep. Prog. Phys. **81**, 016401 (2018).

[11] C. W. von Keyserlingk, V. Khemani, and S. L. Sondhi, Absolute stability and spatiotemporal long-range order in Floquet systems, Phys. Rev. B **94**, 085112 (2016).

[12] V. Khemani, C. W. von Keyserlingk, and S. L. Sondhi, Defining time crystals via representation theory, Phys. Rev. B **96**, 115127 (2017).

[13] K. Sacha, Modeling spontaneous breaking of time-translation symmetry, Phys. Rev. A **91**, 033617 (2015).

[14] N. Y. Yao, A. C. Potter, I.-D. Potirniche, and A. Vishwanath, Discrete Time Crystals: Rigidity, Criticality, and Realizations, Phys. Rev. Lett. **118**, 030401 (2017).

[15] S. Choi, J. Choi, R. Landig, G. Kucsko, H. Zhou, J. Isoya, F. Jelezko, S. Onoda, H. Sumiya, V. Khemani, C. von Keyserlingk, N. Y. Yao, E. Demler, and M. D. Lukin, Observation of discrete time-crystalline order in a disordered dipolar many-body system, Nature (London) **543**, 221 (2017).

[16] J. Zhang, P. W. Hess, A. Kyprianidis, P. Becker, A. Lee, J. Smith, G. Pagano, I.-D. Potirniche, A. C. Potter, A. Vishwanath, N. Y. Yao, and C. Monroe, Observation of a discrete time crystal, Nature (London) **543**, 217 (2017).

[17] A. Chandran and S. L. Sondhi, Interaction-stabilized steady states in the driven $O(N)$ model, Phys. Rev. B **93**, 174305 (2016).

[18] B. Huang, Y.-H. Wu, and W. V. Liu, Clean Floquet Time Crystals: Models and Realizations in Cold Atoms, Phys. Rev. Lett. **120**, 110603 (2018).

[19] S. Pal, N. Nishad, T. S. Mahesh, and G. J. Sreejith, Temporal Order in Periodically Driven Spins in Star-Shaped Clusters, Phys. Rev. Lett. **120**, 180602 (2018).

[20] J. Rovny, R. L. Blum, and S. E. Barrett, Observation of Discrete-Time-Crystal Signatures in an Ordered Dipolar Many-Body System, Phys. Rev. Lett. **120**, 180603 (2018).

[21] S. Autti, V. B. Eltsov, and G. E. Volovik, Observation of a Time Quasicrystal and its Transition to a Superfluid Time Crystal, Phys. Rev. Lett. **120**, 215301 (2018).

[22] C. Chin, R. Grimm, P. Julienne, and E. Tiesinga, Feshbach resonances in ultracold gases, Rev. Mod. Phys. **82**, 1225 (2010).

[23] M. Olshanii, Atomic Scattering in the Presence of an External Confinement and a Gas of Impenetrable Bosons, Phys. Rev. Lett. **81**, 938 (1998).

[24] F. Deuretzbacher, D. Becker, J. Bjerlin, S. M. Reimann, and L. Santos, Quantum magnetism without lattices in strongly interacting one-dimensional spinor gases, Phys. Rev. A **90**, 013611 (2014).

[25] A. G. Volosniev, D. V. Fedorov, A. S. Jensen, M. Valiente, and N. T. Zinner, Strongly interacting confined quantum systems in one dimension, Nat. Commun. **5**, 5300 (2014).

[26] G. M. Koutentakis, S. I. Mistakidis, and P. Schmelcher, Probing ferromagnetic order in few-fermion correlated spin-flip dynamics, arXiv:1804.07199.

[27] M. H. Devoret, A. Wallraff, and J. M. Martinis, Superconducting qubits: A short review, arXiv:cond-mat/0411174.

[28] J. Q. You and F. Nori, Superconducting circuits and quantum information, Phys. Today **58**(11), 42 (2005).

[29] M. H. Devoret and R. J. Schoelkopf, Superconducting circuits for quantum information: An outlook, Science **339**, 1169 (2013).

[30] X. Gu, A. F. Kockum, A. Miranowicz, Y.-x. Liu, and F. Nori, Microwave photonics with superconducting quantum circuits, Phys. Rep. **718–719**, 1 (2017).

[31] I. Buluta and F. Nori, Quantum simulators, Science **326**, 108 (2009).

[32] J. Q. You and F. Nori, Atomic physics and quantum optics using superconducting circuits, Nature (London) **474**, 589 (2011).

[33] U. L. Heras, A. Mezzacapo, L. Lamata, S. Filipp, A. Wallraff, and E. Solano, Digital Quantum Simulation of Spin Systems in Superconducting Circuits, Phys. Rev. Lett. **112**, 200501 (2014).

[34] C. Neill, P. Roushan, K. Kechedzhi, S. Boixo, S. V. Isakov, V. Smelyanskiy, A. Megrant, B. Chiaro, A. Dunsworth, K. Arya, R. Barends, B. Burkett, Y. Chen, Z. Chen, A. Fowler, B. Foxen, M. Giustina, R. Graff, E. Jeffrey, T. Huang, J. Kelly, P. Klimov, E. Lucero, J. Mutus, M. Neeley, C. Quintana, D. Sank, A. Vainsencher, J. Wenner, T. C. White, H. Neven, and J. M. Martinis, A blueprint for demonstrating quantum supremacy with superconducting qubits, Science **360**, 195 (2018).

[35] W. W. Ho, S. Choi, M. D. Lukin, and D. A. Abanin, Critical Time Crystals in Dipolar Systems, Phys. Rev. Lett. **119**, 010602 (2017).

[36] A. Russomanno, F. Iemini, M. Dalmonte, and R. Fazio, Floquet time crystal in the Lipkin-Meshkov-Glick model, Phys. Rev. B **95**, 214307 (2017).

[37] K. Giergiel, A. Kosior, P. Hannaford, and K. Sacha, Time crystals: Analysis of experimental conditions, Phys. Rev. A **98**, 013613 (2018).

[38] A. Kosior and K. Sacha, Dynamical quantum phase transitions in discrete time crystals, Phys. Rev. A **97**, 053621 (2018).

[39] A. G. Volosniev, D. Petrosyan, M. Valiente, D. V. Fedorov, A. S. Jensen, and N. T. Zinner, Engineering the dynamics of effective spin-chain models for strongly interacting atomic gases, Phys. Rev. A **91**, 023620 (2015).

[40] N. Loft, L. Kristensen, A. Thomsen, A. Volosniev, and N. Zinner, CONAN-the cruncher of local exchange coefficients for strongly interacting confined systems in one dimension, Comput. Phys. Commun. **209**, 171 (2016).

[41] F. Deuretzbacher, D. Becker, and L. Santos, Momentum distributions and numerical methods for strongly interacting one-dimensional spinor gases, Phys. Rev. A **94**, 023606 (2016).
[42] N. Y. Yao and C. Nayak, Time crystals in periodically driven systems, Phys. Today **71**(9), 40 (2018).
[43] G. Zürn, F. Serwane, T. Lompe, A. N. Wenz, M. G. Ries, J. E. Bohn, and S. Jochim, Fermionization of Two Distinguishable Fermions, Phys. Rev. Lett. **108**, 075303 (2012).
[44] P. Wicke, S. Whitlock, and N. J. van Druten, Controlling spin motion and interactions in a one-dimensional Bose gas, arXiv:1010.4545.
[45] B. K. Stuhl, H.-I. Lu, L. M. Aycock, D. Genkina, and I. B. Spielman, Visualizing edge states with an atomic Bose gas in the quantum Hall regime, Science **349**, 1514 (2015).
[46] L. Yang and X. Cui, Effective spin-chain model for strongly interacting one-dimensional atomic gases with an arbitrary spin, Phys. Rev. A **93**, 013617 (2016).
[47] E. K. Laird, Z.-Y. Shi, M. M. Parish, and J. Levinsen, SU(N) fermions in a one-dimensional harmonic trap, Phys. Rev. A **96**, 032701 (2017).
[48] G. Pagano, M. Mancini, G. Cappellini, P. Lombardi, F. Schäfer, H. Hu, X.-J. Liu, J. Catani, C. Sias, M. Inguscio, and L. Fallani, A one-dimensional liquid of fermions with tunable spin, Nat. Phys. **10**, 198 (2014).
[49] M. Mancini, G. Pagano, G. Cappellini, L. Livi, M. Rider, J. Catani, C. Sias, P. Zoller, M. Inguscio, M. Dalmonte, and L. Fallani, Observation of chiral edge states with neutral fermions in synthetic Hall ribbons, Science **349**, 1510 (2015).
[50] F. Yan, S. Gustavsson, A. Kamal, J. Birenbaum, A. P. Sears, D. Hover, T. J. Gudmundsen, D. Rosenberg, G. Samach, S. Weber, J. L. Yoder, T. P. Orlando, J. Clarke, A. J. Kerman, and W. D. Oliver, The flux qubit revisited to enhance coherence and reproducibility, Nat. Commun. **7**, 12964 (2016).
[51] S. M. Girvin, M. H. Devoret, and R. J. Schoelkopf, Circuit QED and engineering charge-based superconducting qubits, Phys. Scr. **T137**, 014012 (2009).
[52] M. H. Devoret, Quantum fluctuations in electrical circuits, in *Fluctuations Quantiques/Quantum Fluctuations: Les Houches Session LXIII*, edited by S. Reynaud, E. Giacobino, and J. Zinn-Justin (Elsevier, Amsterdam, 1997), p. 351.
[53] U. Vool and M. H. Devoret, Introduction to quantum electromagnetic circuits, Int. J. Circuit Theory Appl. **45**, 897 (2017).
[54] P. Rebentrost and F. K. Wilhelm, Optimal control of a leaking qubit, Phys. Rev. B **79**, 060507(R) (2009).
[55] N. Khaneja, T. Reiss, C. Kehlet, T. Schulte-Herbrüggen, and S. J. Glaser, Optimal control of coupled spin dynamics: Design of NMR pulse sequences by gradient ascent algorithms, J. Magn. Reson. **172**, 296 (2005).
[56] F. Motzoi, J. M. Gambetta, P. Rebentrost, and F. K. Wilhelm, Simple Pulses for Elimination of Leakage in Weakly Nonlinear Qubits, Phys. Rev. Lett. **103**, 110501 (2009).
[57] J. R. Johansson, P. D. Nation, and F. Nori, Qutip 2: A Python framework for dynamics of open quantum systems, Comput. Phys. Commun. **184**, 1234 (2013).
[58] W. C. Yu, J. Tangpanitanon, A. W. Glaetzle, D. Jaksch, and D. G. Angelakis, Discrete time crystal in globally driven interacting quantum systems without disorder, Phys. Rev. A **99**, 033618 (2019).
[59] F. Deuretzbacher, K. Fredenhagen, D. Becker, K. Bongs, K. Sengstock, and D. Pfannkuche, Exact Solution of Strongly Interacting Quasi-One-Dimensional Spinor Bose Gases, Phys. Rev. Lett. **100**, 160405 (2008).
[60] I. Bloch, Ultracold quantum gases in optical lattices, Nat. Phys. **1**, 23 (2005).
[61] J. Koch, T. M. Yu, J. Gambetta, A. A. Houck, D. I. Schuster, J. Majer, A. Blais, M. H. Devoret, S. M. Girvin, and R. J. Schoelkopf, Charge-insensitive qubit design derived from the Cooper pair box, Phys. Rev. A **76**, 042319 (2007).
[62] R. Barends, J. Kelly, A. Megrant, D. Sank, E. Jeffrey, Y. Chen, Y. Yin, B. Chiaro, J. Mutus, C. Neill, P. O'Malley, P. Roushan, J. Wenner, T. C. White, A. N. Cleland, and J. M. Martinis, Coherent Josephson Qubit Suitable for Scalable Quantum Integrated Circuits, Phys. Rev. Lett. **111**, 080502 (2013).
[63] T. P. Orlando, J. E. Mooij, L. Tian, C. H. van der Wal, L. S. Levitov, S. Lloyd, and J. J. Mazo, Superconducting persistent-current qubit, Phys. Rev. B **60**, 15398 (1999).
[64] J. E. Mooij, T. P. Orlando, L. Levitov, L. Tian, C. H. van der Wal, and S. Lloyd, Josephson persistent-current qubit, Science **285**, 1036 (1999).
[65] C. H. van der Wal, A. C. J. ter Haar, F. K. Wilhelm, R. N. Schouten, C. J. P. M. Harmans, T. P. Orlando, S. Lloyd, and J. E. Mooij, Quantum superposition of macroscopic persistent-current states, Science **290**, 773 (2000).
[66] V. E. Manucharyan, J. Koch, L. I. Glazman, and M. H. Devoret, Fluxonium: Single Cooper-pair circuit free of charge offsets, Science **326**, 113 (2009).
[67] A. J. Berkley, H. Xu, R. C. Ramos, M. A. Gubrud, F. W. Strauch, P. R. Johnson, J. R. Anderson, A. J. Dragt, C. J. Lobb, and F. C. Wellstood, Entangled macroscopic quantum states in two superconducting qubits, Science **300**, 1548 (2003).
[68] W. S. Warren, Effects of arbitrary laser or NMR pulse shapes on population inversion and coherence, J. Chem. Phys. **81**, 5437 (1984).
[69] M. Steffen, J. M. Martinis, and I. L. Chuang, Accurate control of Josephson phase qubits, Phys. Rev. B **68**, 224518 (2003).